Miniaturization Techniques Using Magnetic Materials for Broadband Antenna Applications

Ravi Durbha and Mohammed N. Afsar, *Life Fellow, IEEE*

Department of Electrical and Computer Engineering, Tufts University, Medford, MA 02155 USA

This paper investigates the instrumentation necessary to analyze frequency-dependent complex parameters of solid magnetic materials based on T/R-based waveguide measurement technique proposed by W. B. Weir. Based on the magnitude and phase values of transmission and reflection coefficients measured using vector network analyzer, complex permittivity and permeability are calculated using the expressions defined. Equations necessary for calculating the complex parameters as a function of frequency with required step size are derived from the experimental results. To validate mathematical expressions developed for composite magnetic materials, the design of a compact 2–18 GHz cavity-backed spiral antenna using off-the-shelf magnetic materials is presented. The electrical performance of the cavity along with stack of high contrast magnetic materials of varying dimensions is modeled and simulated in ANSYS HFSS software.

Index Terms—**Cavity-backed spiral antenna, ferro-magnetic materials, Klopfenstein taper, permeability, permittivity.**

I. Introduction

WITH advancements in signal processing techniques, the present trend in the development of miniaturized components is implementing the concept of SWAP, i.e., reduction in size, weight, and power without degrading the electrical performance of the system. Advancements in the technology development of antennas for various commercial and military applications are no exceptional. The aperture size of antennas is often limited due to size restrictions dictated by the platform on which they are installed. For this reason, these antennas are required to be compact and retain their electrical performance without any variation. Structural compactness can be achieved by loading the antenna with absorbing material. Two properties of fundamental interest in the application of ferrites at microwave frequencies are the dielectric and magnetic susceptibilities, i.e., permittivity and permeability. The presence of a magnetized ferrite in a cavity normally causes a change of Q of the cavity and a shift in the resonant frequency [1], which leads to increase in operating bandwidth without increasing the size of the antenna aperture. The main reason for this phenomenon is dampening of cavity resonance as described in [2] and [3]. Therefore, suitable absorbing materials with varying attenuation characteristics over the frequency band are to be designed. Permittivity and permeability are the function of frequency and designing an absorber with varying absorption coefficients spread across a wide spectrum of frequency is complicated. As a result, most homogeneous absorbing materials are effectively narrowband absorbers.

The best possible solution to this problem is to stack multiple absorbing layers into a composite structure and tune the thickness of each layer so that an overall broadband response is obtained. In this paper, the transmission-reflection-based waveguide measurement technique is implemented to accurately calculate permittivity and permeability of various off-the-shelf available ferrite absorbers over a wide frequency spectrum. To exploit the effectiveness of the absorber so characterized based on the measured complex data, a compact cavity-backed archimedean spiral antenna operating in the frequency range 2–18 GHz is designed and characterized using the finite-element method-based electromagnetic (EM) simulation tool ANSYS HFSS.

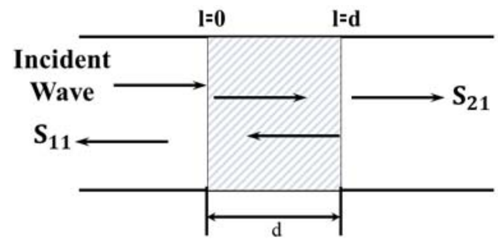

Fig. 1. Schematic of sample material in waveguide.

II. Theory of Dielectric Material Characterization

In this paper, a method for broadband simultaneous measurement of transmission and reflection (T/R) parameters using vector network analyzer developed by Weir [4] is implemented for characterizing complex permittivity and permeability values of ferrite materials. The measurements are carried out in the frequency range of 2–18 GHz. The frequency range is sub-divided into bands, i.e., L-band (1.7–2.6 GHz), S-band (2.6–3.95 GHz), G-band (3.95–5.85 GHz), C-band (5.85–8.2 GHz), X-band (8.2–12.4 GHz), and Ku-band (12.4–18 GHz).

In waveguide measurement technique, the standard two-port thru, reflect, and load calibration applies to zero reference plane findings to have minimum insertion loss. EM wave propagating with dielectric material loaded inside the waveguide fixed onto the zero reference plane is as shown in Fig. 1.

Manuscript received November 4, 2018; revised December 24, 2018; accepted January 14, 2019. Date of publication April 1, 2019; date of current version June 20, 2019. Corresponding author: R. Durbha (e-mail: ravi.durbha@tufts.edu).

Color versions of one or more of the figures in this paper are available online at http://ieeexplore.ieee.org.

Digital Object Identifier 10.1109/TMAG.2019.2894644

When EM wave is incident on the sample placed inside the waveguide, some of the energy is reflected back and some transmitted through the medium. Reflection and transmission coefficients can be derived from measured values of S_{11} and S_{21} by the following equations [5]:

$$S_{11} = \frac{[1 - T^2]\Gamma}{1 - T^2\Gamma^2} \tag{1}$$

$$S_{21} = \frac{[1 - \Gamma^2]T}{1 - T^2\Gamma^2}. \tag{2}$$

Propagation constant for a wave propagating through the material is defined as

$$T = e^{-\gamma d} = e^{-(\alpha + j\beta)d} \tag{3}$$

where γ is the propagation constant, α is the attenuation constant, and β is the phase constant.

From (1) and (2), reflection coefficient (Γ) and transmission coefficient (T) can be written as

$$\Gamma = K \pm \sqrt{K^2 - 1} \tag{4}$$

where

$$K = \frac{S_{11}^2 - S_{21}^2 + 1}{2S_{11}} \tag{5}$$

and

$$T = \frac{S_{11} + S_{21} - \Gamma}{1 - (S_{11} + S_{21})\Gamma}. \tag{6}$$

From (3), propagation constant for dominant mode of propagation can be written as

$$\Upsilon_{\mathrm{TE}_{10}} = \frac{1}{d}\ln\left(\frac{1}{|T|}\right). \tag{7}$$

The transmission coefficient T defined in (7) is a complex number, there are multiple values for Υ. If T is defined as

$$T = |T|e^{j\emptyset}. \tag{8}$$

Then, Υ is given by

$$\Upsilon_{\mathrm{TE}_{10}} = \frac{1}{d}\ln\left(\frac{1}{|T|}\right) + j\left(\frac{2\pi n - \varphi_T}{d}\right). \tag{9}$$

Normally, the thickness (d) of the sample loaded inside the waveguide should be less than a quarter wavelength because it will make $n = 0$. In order to compute permittivity and permeability of the given sample, Maxwell equations are solved by substituting boundary conditions.

The propagation constant of TE_{10} can be subsequently be written as in [6]

$$\Upsilon_{\mathrm{TE}_{10}} = j2\pi\sqrt{\left(\frac{1}{\lambda_o}\right)^2 - \left(\frac{1}{2a}\right)^2} \times \sqrt{\mu\varepsilon} = j\Upsilon^0_{\mathrm{TE}_{10}}\frac{\mu}{\eta}$$

where

$$\Upsilon^0_{\mathrm{TE}_{10}} = 2\pi\sqrt{\left(\frac{1}{\lambda_o}\right)^2 - \left(\frac{1}{2a}\right)^2}. \tag{10}$$

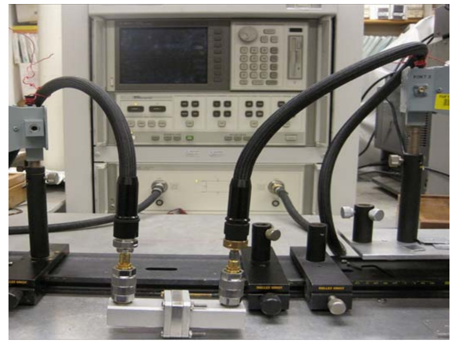

Fig. 2. Experimental setup for magnetic material characterization.

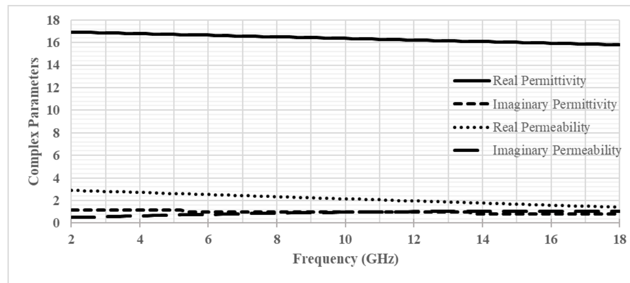

Fig. 3. Complex permittivity and permeability of MF116 material.

The complex permeability and permittivity associated with propagation constant are expressed as

$$\mu = \frac{\eta\Upsilon_{\mathrm{TE}_{10}}}{j\Upsilon^0_{\mathrm{TE}_{10}}} = -j\left(\frac{1+\Gamma}{1-\Gamma}\right)\left(\frac{1}{2\pi d}\right) \times \left(\frac{\ln\left(\frac{1}{|T|}\right) + j(2\pi n - \varphi_T}{\sqrt{\left(\frac{1}{\lambda_0}\right)^2 - \left(\frac{1}{2a}\right)^2}}\right) \tag{11}$$

$$\varepsilon = \frac{\mu}{Z_{TE}^2} = \frac{\mu}{\eta^2}\left(\lambda_0^2\left(\frac{1}{\lambda_0^2} - \frac{1}{4a^2}\right)\right) \tag{12}$$

where

$$\eta = (1+\Gamma)/(1-\Gamma)$$

$$\varepsilon = -j\left(\frac{c}{f}\right)^2\left(\frac{1-\Gamma}{1+\Gamma}\right)\left(\frac{1}{2\pi d}\right)\left(\ln\left(\frac{1}{|T|}\right) + j(2\pi n - \varphi_T)\right) \times \left(\sqrt{\left(\frac{1}{\lambda_0}\right)^2 - \left(\frac{1}{2a}\right)^2}\right). \tag{13}$$

Equations (12) and (13) are used to calculate complex permeability and permittivity values. The experimental setup of waveguide measurement shown in Fig. 2 is implemented to characterize Eccosorb MF116, and MF117 sample materials from Liard Tech [7] the results are as shown in Figs. 3 and 4.

By implementing curve fitting method using MATLAB software mathematical expressions defining the relation between complex parameters as a function of frequency is obtained. The derived equations for the two materials used are given from (14) through (21), where f is the frequency in gigahertz.

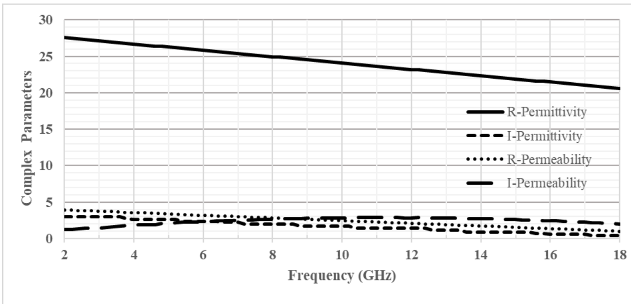

Fig. 4. Complex permittivity and permeability of MF117 material.

For MF116

$$\begin{aligned}
\varepsilon' &= -0.000001012f^2 - 0.07061f + 17.0711 &(14)\\
\tan\delta_d &= 0.0000067f^2 - 0.001481f + 0.073376 &(15)\\
\mu' &= 0.0096242f^2 - 0.28892f + 3.5427 &(16)\\
\tan\delta_m &= -0.0026619f^2 + 0.093632f + 0.074767. &(17)
\end{aligned}$$

For MF117

$$\begin{aligned}
\varepsilon' &= -0.00000156f^2 - 0.4353f + 28.4329 &(18)\\
\tan\delta_d &= 0.00042939f^2 - 0.011194f + 0.090549 &(19)\\
\mu' &= 0.020754f^2 - 0.57571f + 4.8921 &(20)\\
\tan\delta_m &= -0.0056458f^2 + 0.22112f - 0.19616 &(21)
\end{aligned}$$

where ε' is the real part of permittivity of dielectric material, $\tan\delta_d$ is the dielectric loss tangent, μ' is the real part of permeability of dielectric material, and $\tan\delta_m$ is the magnetic loss tangent.

For simplicity, quadratic polynomial is used for data curve fitting. A variation of about 5%–8% in the values of the complex data is observed by using quadratic expressions derived. This variation can be minimized using higher order polynomial expressions.

III. Design of Cavity-Backed Spiral Antenna

For any antenna, physical dimension is the key constraint which limits and defines important electrical parameters such as bandwidth of operation, beamwidth, and gain. Magnetic materials play an important role in minimizing the effort required to miniaturize the size of the antenna without degrading the electrical performance. By loading the cavity with carefully characterized magnetic material with appropriate dimensions back radiation in the cavity and electrical parameters in the boresight can be optimized.

In this section, the design of a cavity-backed spiral antenna loaded with MF116 and MF117 in conjunction with materials such as Teflon and hard rubber which are used as spacers is presented. A self-complimentary Archimedean spiral antenna [8] is shown in Fig. 5.

For an Archimedean spiral antenna fabricated on a dielectric material such as polytetrafluoroethylene (PTFE), input impedance varies as a function of dielectric constant ε_r and is given as

$$Z_{\text{in}} = \frac{\eta}{2\sqrt{\varepsilon_r}} = \frac{188.5}{\sqrt{\varepsilon_r}}\ \Omega \qquad (22)$$

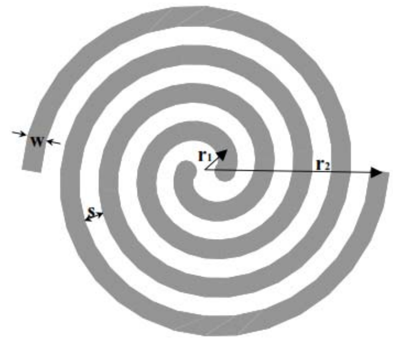

Fig. 5. Geometry of Archimedean spiral antenna.

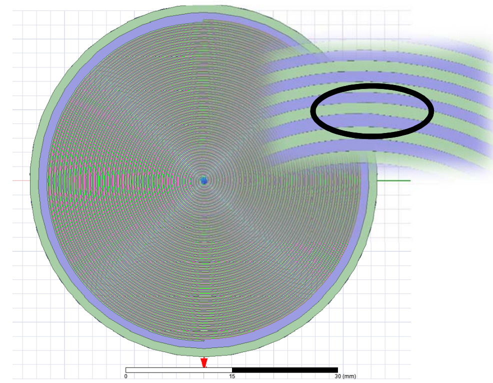

Fig. 6. Geometry of parameterized Archimedean spiral antenna generated in HFSS.

η – free space impedance = 120π = 377 ohms.

Each arm of the spiral is linearly proportional to angle Ø, i.e., rate of growth and is defined as given in the following:

$$\begin{aligned}
r &= r_o\phi + r_1\\
r &= r_o(\theta - \pi) + r_1 \qquad (23)
\end{aligned}$$

where r_1 is the inner radius of the spiral antenna, r_o is the proportionality constant and is given as

$$r_o = \frac{S+W}{\pi} = \frac{2W}{\pi}. \qquad (24)$$

For a self-complementary archimedean with N-turns spiral spacing (S) and width (W) is equal and they can be determined from

$$S = W = \frac{r_2 - r_1}{4N}. \qquad (25)$$

Based on the above-mentioned theory, the lowest operating frequency of the spiral is theoretically determined by the outer radius and the highest operating frequency defines the feed point spacing expressed as

$$\begin{aligned}
f_{\text{low}} &= \frac{c}{2\pi r_2}\\
f_{\text{high}} &= \frac{c}{2\pi r_1} \qquad (26)
\end{aligned}$$

where c is the velocity of light in free space = 3×10^8 m/sec.

The minimum diameter required for the spiral antenna to radiate into free space is λ/π, which is, much less than the actual diameter of the spiral antenna. Therefore, the concept

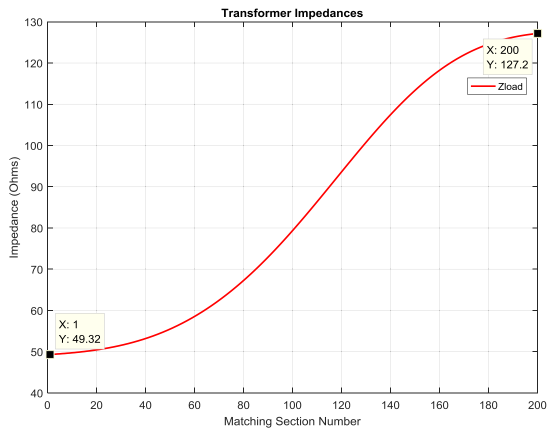

Fig. 7. Variation in impedance with respect to the number of sections of taper.

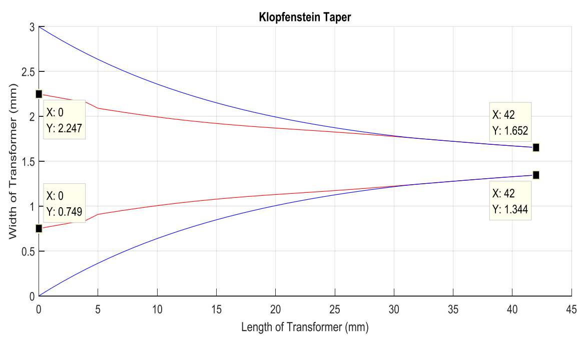

Fig. 8. Klopfenstein taper artwork.

miniaturization emanates. Fig. 6 shows a simple design of the compact antenna with tapered arm width [8], modeled in ANSYS HFSS. Improper excitation of spiral antenna gives rise to pattern asymmetry and pattern squint. The equations proposed in [9] and [10] provide broadband impedance matching of balun by matching non-uniform lines of unequal impedances over a frequency range of 2–18 GHz as shown in Figs. 7 and 8.

The length of the taper is determined by the lowest operating frequency and the maximum reflection coefficient defined in the pass band. The balun has no upper frequency limit other than the frequency where higher order coaxial modes are supported or where radiation from the open wire line becomes appreciable. For the maximum bandwidth with a fixed max magnitude of reflection coefficient then, the input reflection coefficient for a continuous line taper is given by

$$\rho = \rho_o e^{-j\beta l}\left[\frac{\cos\sqrt{(\beta l)^2 - A^2}}{\cosh(A)}\right] \tag{27}$$

where A is the maximum magnitude of the reflection coefficient in the pass band, β is defined as phase constant, and l is the length of transmission line. The reflection coefficient magnitude takes on its maximum value ρl at zero frequency, and will oscillate in the pass band with constant amplitude equal to $\rho_o/\cosh A$. By taking inverse Fourier transform of (17), the incremental reflection coefficient at each cross section

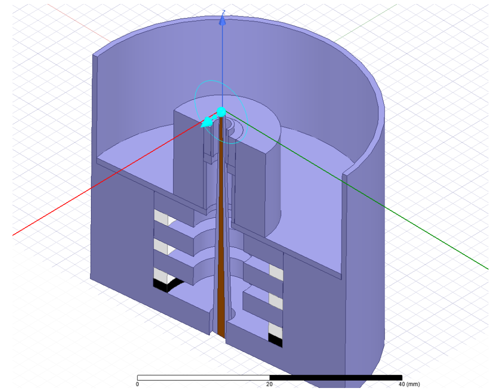

Fig. 9. Taper simulation setup inside dielectric loaded cavity.

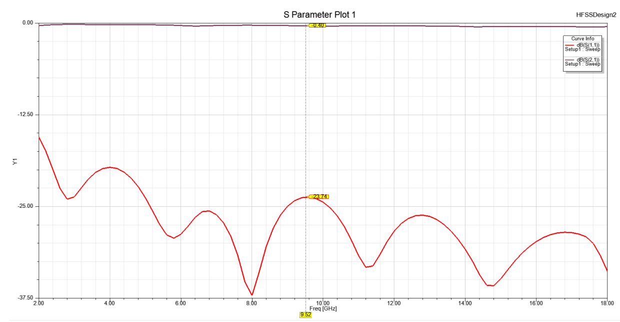

Fig. 10. Simulated results of taper inside dielectric loaded cavity.

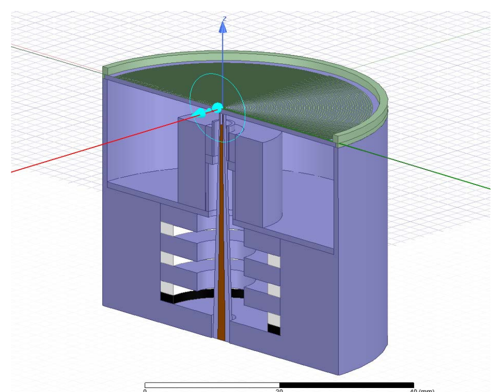

Fig. 11. Sectional view of the cavity backed spiral antenna.

is given by

$$F(X) = \left(\frac{\rho_o}{\cosh(A)}\right)\left\{\left(\frac{A^2}{l}\right)\frac{I_1\left[A\sqrt{1-\left(\frac{2X}{l}\right)^2}\right]}{A\sqrt{1-\left(\frac{2X}{l}\right)^2}} + \frac{1}{2}\left[\delta\left(x-\frac{l}{2}\right)+\delta\left(x+\frac{l}{2}\right)\right]\right\} \quad |X| \le l/2$$

$$= 0 \quad |X| \ge l/2 \tag{28}$$

where I_1 is the first kind of modified Bessel function of the first order, and δ is the unit impulse function.

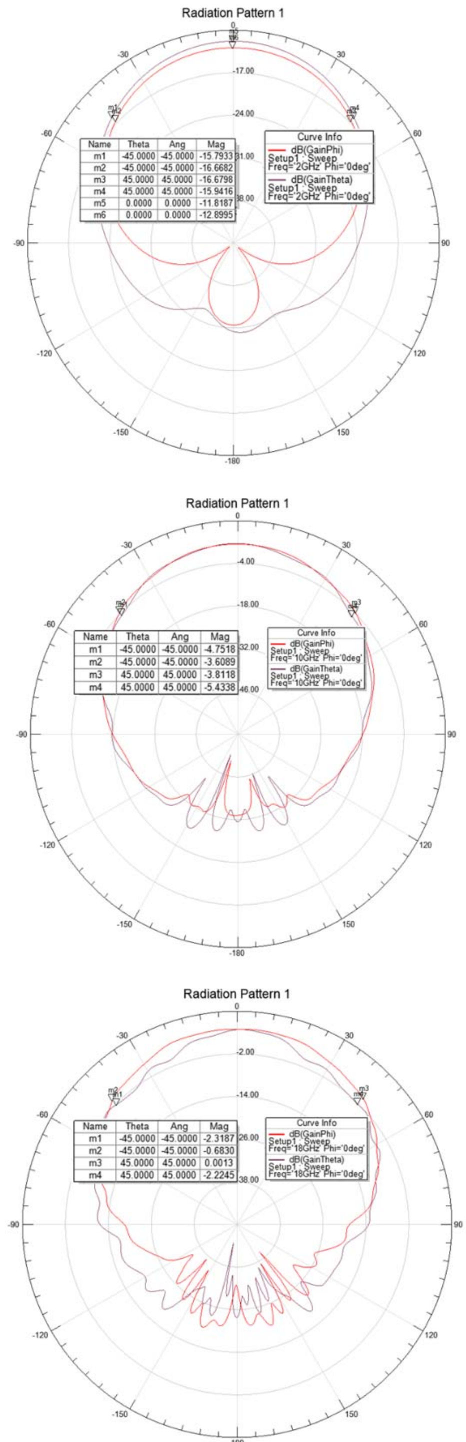

Fig. 12. Radiation patterns in 0° cut plane across the frequency range 2–18 GHz.

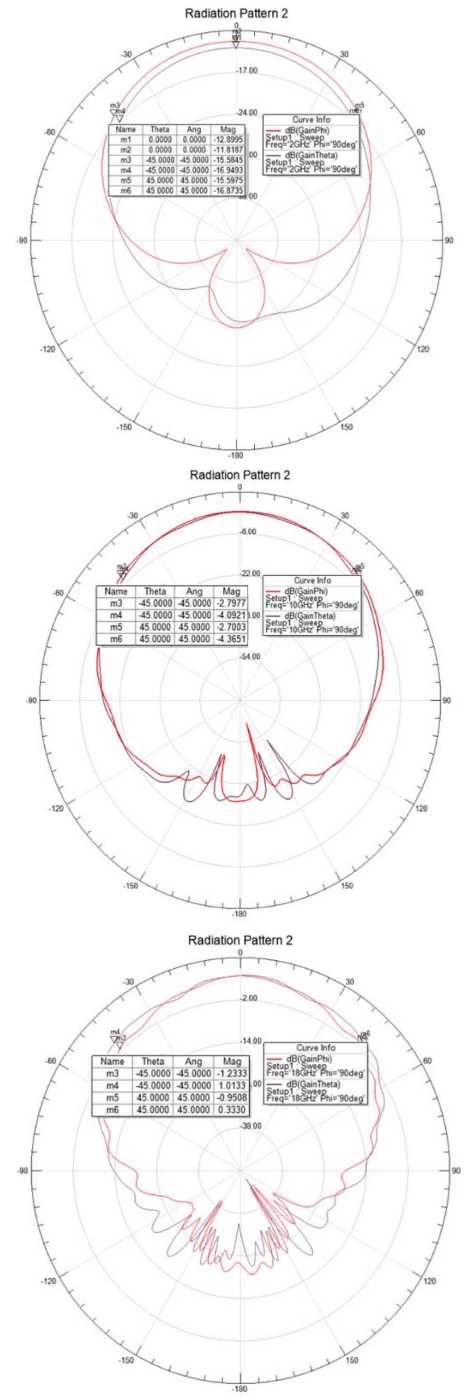

Fig. 13. Radiation patterns in 90° cut plane across the frequency range 2–18 GHz.

Reflection coefficient is defined as

$$\rho_o = \left(\frac{1}{2}\right) \ln\left(Z_2/Z_1\right). \tag{29}$$

The variation in characteristic impedance along the taper can be found by direct integration of F(X), and it is given by

$$\begin{aligned} \ln(Z_o) &= \frac{1}{2}\ln(Z_1 Z_2) \\ &\quad + \frac{\rho_o}{\cosh(A)}\left\{A^2\phi(2x/l, A) + U\left(x - \frac{l}{2}\right)\right. \\ &\quad \left. + U\left(x + \frac{l}{2}\right)\right\} \quad |x| \le l/2 \\ &= \ln(Z_2), \quad x > \frac{l}{2} \\ &= \ln(Z_1), \quad x < \frac{-l}{2} \end{aligned} \tag{30}$$

where U is the unit step function defined by

$$\begin{aligned} U(z) &= 0, \quad z < 0 \\ U(z) &= 1, \quad z \ge 0 \end{aligned} \tag{31}$$

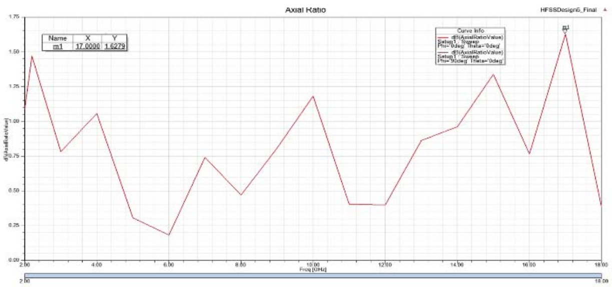

Fig. 14. Axial ratio in boresight over the frequency range 2–18 GHz.

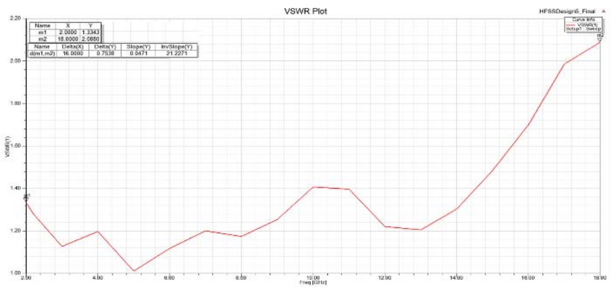

Fig. 15. Simulated response of VSWR over the frequency range 2–18 GHz.

Φ is defined by

$$\phi(z, A) = -\phi(-z, A) = \int_0^z \frac{I_1(A\sqrt{1-y^2})}{A\sqrt{1-y^2}} dy \quad \text{For } |z| \leq 1. \tag{32}$$

Equation (30) represents the Dolph–Chebyshev tapered transition. Z_1 is the input impedance of 50 Ω and Z_2 represents the input impedance of the antenna to which the taper is matched. While Z_o represents the characteristic impedance of the transmission line taper and z represents the location of calculating the impedance.

MATLAB routines are developed using (27) through (32) to study the variation in impedance with respect to the number of sections required to design a taper which has impedance matching over the frequency range of 2–18 GHz is shown in Figs. 7 and 8. The generated artwork is imported into 3-D simulation and modeled on a 20 mil thick double-sided copper cladded PTFE material from Rogers Corporation as shown in Fig. 9. Simulated results of taper with return loss better than −10 dB and insertion loss no greater than 1.0 dB across the required impedance bandwidth is shown in Fig. 10. To nullify the back radiation of the antenna, the spiral antenna is placed inside a metallic cavity. The study of effect of cavity height is analogs to placing of dipole over ground plane [10].

The initial height of the cavity is assumed to integral multiple of half-wavelength at the lowest operating frequency. The height of the cavity is optimized by loading the cavity with magnetic material of high contrast permeability and permittivity to minimize internal reflections of EM-wave across the bandwidth of operation. Fig. 11 shows the sectional view of the dielectric loaded cavity-backed spiral antenna modeled in ANSYS HFSS to evaluate EM performance.

TABLE I
COMPARISON OF AXIAL RATIO IN BORESIGHT AND OFF-AXIS (±45°) ACROSS THE FREQUENCY RANGE

S.No.	**Freq. (GHz)**	**Axial Ratio**		
		Boresight (0°)	**Off-Axis (-45°)**	**Off-Axis (+45°)**
1	2	1.08	0.04	0.07
2	4	1.05	0.13	0.07
3	6	0.18	0.24	0.12
4	8	0.47	0.82	0.2
5	10	1.18	0.74	1.1
6	12	0.40	0.09	0.61
7	14	0.96	3.44	2.94
8	16	0.77	1.91	1.8
9	18	0.38	1.39	0.8

TABLE II
COMPARISON OF GAIN, BEAMWIDTH IN $\Phi = 0°$ AND 90° PLANE ACROSS THE FREQUENCY RANGE

S.No.	**Frequency (GHz)**	**Gain (dB)**	**Beamwidth (deg.)**	
			VP	**HP**
1	2	-9.31	78.55	79.16
2	4	1.66	79.76	81.4
3	6	1.70	59.81	60.56
4	8	2.04	62.34	67.5
5	10	5.4	57.03	62.45
6	12	4.05	83.56	85.5
7	14	3.06	85.26	108.43
8	16	6.22	72.06	63.84
9	18	7.90	50.77	54.63

IV. RESULTS

From the initial study of design of the cavity-backed spiral antenna without dielectric loading, deviations in electrical performance were observed. By loading the cavity with only one absorbing material, there was not much improvement in the electrical performance of the antenna. Therefore, the cavity is loaded with stackup of magnetic material with optimized dimensions and analyzed for EM performance. From the simulated results presented, it can be observed that stackup of magnetic material provides more degrees of freedom for optimizing electrical parameters of the antenna. The results so obtained are described in the following.

Table I illustrates the data of the on-axis axial ratio, i.e., at boresight which is $\leq$3 dB and off-axis axial ratio, i.e., at $\pm 45^\circ$ is $\leq$4 dB. The off-axis axial ratio data are one of the important parameters for consideration in design of antenna array for electronic warfare applications. Table II summarizes the gain and beamwidth of the simulated antenna in both $\Phi = 0^\circ$ and 90° planes, which vary in the range of 50° (min.) and 110° (max.) across the frequency spectrum. Figs. 12 and 13 show the radiation patterns along with front-to-back ratio (FBR) <-10 dB of across antenna operating bandwidth. Figs. 14 and 15 describe the information about axial ratio of antenna at boresight and simulated VSWR across 2–18 GHz frequency band. It can be concluded that the results so obtained from the simulation show that the antenna has better electrical performance in terms of axial ratio, beamwidth, and FBR.

V. Conclusion

Characterization of solid magnetic materials along with necessary instrumentation and equations for frequency-dependent complex parameters is presented. Design of a compact and efficient wideband spiral antenna with a diameter approximately 50 mm is characterized. While retaining compact size, other electrical parameters such as FBR ≤ -10 dB, axial ratio $\leq$3 dB in boresight, and $\leq$4 dB off-axis, i.e., $\pm 45^\circ$ and VSWR < 2.5 across the operating frequency bandwidth is achieved. The antenna so designed operates reliably while retaining the system performance with constraints set by the platform on which it is installed. Such compact antennas with near circular polarization find applications as baseline interferometry arrays in direction finding receivers.

References

[1] B. Lax and K. Button, *Microwave Ferrites and Ferrimagnetics*. New York, NY, USA: McGraw-Hill, 1962, pp. 323–324.
[2] P. Dixon, “Cavity-resonance dampening,” *IEEE Microw. Mag.*, vol. 6, no. 2, pp. 74–84, Jul. 2005.
[3] A. Sundsmo, “Microwave absorbers: Reducing cavity resonances,” Appl. Note, 2006. [Online]. Available: http://www.masttechnologies.com/application-notes
[4] W. B. Weir, “Automatic measurement of complex dielectric constant and permeability at microwave frequencies,” *Proc. IEEE*, vol. 62, no. 1, pp. 33–36, Jan. 1974.
[5] D. K. Ghodgaonkar, V. V. Varadan, and V. K. Varadan, “Free-space measurement of complex permittivity and complex permeability of magnetic materials at microwave frequencies,” *IEEE Trans. Instrum. Meas.*, vol. 39, no. 2, pp. 387–394, Apr. 1990.
[6] N. N. Al-Moayed, M. N. Afsar, U. A. Khan, S. McCooey, and M. Obol, “Nano ferrites microwave complex permeability and permittivity measurements by T/R technique in waveguide,” *IEEE Trans. Magn.*, vol. 44, no. 7, pp. 1768–1772, Jul. 2008.
[7] Liard Tech. *Eccosorb MF-116, MF-117 Data Sheet*. Accessed: Nov. 21, 2018. [Online]. Available: http://www.eccosorb.com/Collateral/Documents/English-US/RFP-DS-MF%20092115.pdf
[8] R. A. Poisel, *Antenna Systems and Electronic Warfare Applications*. Norwood, MA, USA: Artech House, 2012, pp. 464–467.
[9] M. A. Grossberg, “Extremely rapid computation of the Klopfenstein impedance taper,” *Proc. IEEE*, vol. 56, no. 9, pp. 1629–1630, Sep. 1968.
[10] R. Bawer and J. Wolfe, “The spiral antenna,” in *Proc. IRE Int. Conv. Rec.*, vol. 8, 1960, pp. 84–95.